A Joint Photoelectron Imaging Spectroscopic and Theoretical Characterization on the Electronic Structures of the Anionic and Neutral ZrC2 Clusters.

ARTICLE *in* THE JOURNAL OF PHYSICAL CHEMISTRY A · AUGUST 2014

Impact Factor: 2.69 · DOI: 10.1021/jp505648u · Source: PubMed

2 AUTHORS, INCLUDING:

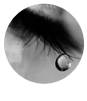

Shibo Cheng
Pennsylvania State University
19 PUBLICATIONS **75** CITATIONS

SEE PROFILE

THE JOURNAL OF PHYSICAL CHEMISTRY A

Article

pubs.acs.org/JPCA

Joint Photoelectron Imaging Spectroscopic and Theoretical Characterization on the Electronic Structures of the Anionic and Neutral ZrC_2 Clusters

Shi-Bo Cheng[†] and A. W. Castleman, Jr.*[,†,‡]

[†]Department of Chemistry and [‡]Department of Physics, The Pennsylvania State University, University Park, Pennsylvania 16802, United States

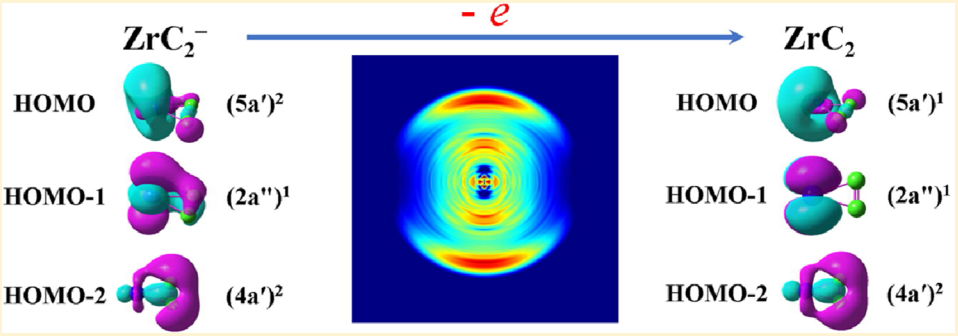

ABSTRACT: We present a joint photoelectron imaging spectroscopic and theoretical investigation on the triatomic ZrC_2^- anion. Vibrationally resolved spectrum was acquired at 532 nm photon energy. Electron affinity for the neutral ZrC_2 cluster was determined to be 1.60 ± 0.07 eV. The CCSD(T) level of theory was used to explore the ground-state geometries and vibrational frequencies of the anionic and neutral ZrC_2 clusters. Our vibrationally resolved photoelectron spectrum reveals two vibrational frequencies (564.6 and 1774.0 cm^{-1}) of the neutral ZrC_2 cluster, which correspond to the symmetric Zr−C_2 and C−C stretching modes, and these experimental findings are in good agreement with the calculated values. Additionally, the molecular orbitals and chemical bonding in the anionic and neutral ZrC_2 clusters are also discussed to disclose the interaction between the transition metal atom (Zr) and C_2 unit.

1. INTRODUCTION

Over the past several decades the interaction between transition metals and carbon has attracted much attention owing to the fact that the transition-metal carbides are believed to have potential applications in the formation of modern materials, including metallofullerene,[1,2] metallocarbohedrenes (met-cars),[3−5] and carbon nanotube.[6] Specifically, met-cars are a new class of unusually stable gas-phase metal carbon cluster ions with a M_8C_{12} stoichiometry, which were discovered in our laboratory in the early 90s.[3−5] Subsequently, extensive investigations were accelerated to explore the electronic structures, reactivity, stability, and delayed ionization of these met-cars and substituted met-cars.[7−14] Additionally, transition metal carbides are also characterized by many unique and intriguing catalytic properties.[15] More interesting, the catalytic properties of some transition metal carbides are found to display similarity to those of the more expensive Pt-group metals.[15] It is well-accepted that the nature of the chemical bonding and electronic structures involved in the metal carbide clusters depend significantly on the nature of different metal atoms. Investigations on small metal−carbon clusters, therefore, can provide ideal and effective models for obtaining a comprehensive understanding of the interaction between metals and carbon, which will help in gaining insight in the growth mechanisms of different metal−carbon nanomaterials as well as in alerting the chemical properties of the transition metal carbides surface.

Compared with a large number of investigations on the first-row (3d) transition-metal carbides,[16−21] the knowledge about the electronic structures of 4d transition-metal carbides are relatively limited. Experimentally, Morse and co-workers have studied the electronic structures of the ground and excited states of PdC employing the resonant two-photon ionization spectroscopy.[22] By trapping nascent sliver−carbon clusters in solid Ar matrix at 12 K, Wang et al. have determined two new infrared frequencies (1827.8 and 1231.6 cm^{-1}) of near-liner AgC_3 by combining the infrared spectroscopy and density functional theory calculations.[23] Additionally, anion photoelectron spectroscopy (PES) was also utilized to explore the electronic states and geometries of some mononiobium and triniobium carbide clusters, which are NbC_n^- (n = 2−7) and $Nb_3C_n^-$ (n = 5−10).[24,25] Recently, Knappenberger et al. have examined the evolving electronic and geometric properties of diniobium carbide clusters, and it was suggested that, for cluster

Received: June 6, 2014
Revised: August 6, 2014
Published: August 6, 2014

dx.doi.org/10.1021/jp505648u | J. Phys. Chem. A 2014, 118, 6935−6939

sizes between Nb_2C_7 and Nb_2C_9, the behavior directly mimics that of pure carbon, in support of niobium substitution of carbon.[26]

In this study, we present vibrationally resolved photoelectron imaging spectroscopy, which has been proven to be a powerful technique to directly detect the electronic characters of atoms and clusters,[27−37] of a small triatomic ZrC_2^- anion. High-level theoretical calculations were also performed to assist in determining the ground-state structures of the anionic and neutral ZrC_2 clusters. Electron affinity (EA) and vibrational frequencies of the neutral ZrC_2 cluster are reported by analyzing the vibrationally resolved PES. Finally, the molecular orbitals and chemical bonding in the clusters are also discussed.

2. EXPERIMENTAL DETAILS

The details of the experimental setup for the current study have been described previously.[38,39] In brief, in the laser vaporization supersonic cluster beam source, the ZrC_2^- cluster was produced by ablating a 1/4″ pure zirconium rod using a second harmonic (532 nm) output of a Nd:YAG laser. A high-purity helium gas (typically 50 psi) seeded with 10% CH_4 gas was used as a carrier gas, which also provides the carbon source to form the desired cluster. The resulting anions were then extracted and mass analyzed employing a Wiley−McLaren time-of-flight mass spectrometer.[40] The mass-selected ZrC_2^- cluster was photodetached by another second harmonic (532 nm) output of a Nd:YAG laser in the laser detachment region, from which the resultant photoelectrons were electronically pushed toward a detector consisting of a 40 mm diameter microchannel plate (MCP) and a phosphor screen. A charge-coupled device camera was used to collect the images formed on the phosphor screen. Subsequently, all the photoelectron images were reconstructed by using both the BASEX[41] and pBASEX[42] programs, which yield similar results. The photoelectron spectrum was calibrated against the known spectroscopic data of Bi^-.[43]

3. COMPUTATIONAL METHODS

In order to aid in both the assignment of the PES and the determination of optimized geometries and electronic structures, high-level ab initio theoretical calculations were carried out on the interested clusters. All calculations presented here were accomplished using the Gaussian 09 program.[44] The anionic and neutral ZrC_2 clusters were optimized employing the coupled cluster singles and doubles with perturbative contributions of connected triplets, CCSD(T) level of theory.[45,46] In the calculations, the atomic orbital of carbon was described by the standard augmented correlation consistent triple-ζ (aug-cc-pvtz) basis set.[47,48] As for Zr atom, the aug-cc-pvtz-pp basis set was used, including small-core energy-consistent relativistic pseudopotentials (PP) to account for the relativistic effects.[49] To determine the lowest energy geometries of the clusters, various initial geometries and spin multiplicity states were calculated and fully optimized without symmetry constraints. The frequency calculations were also performed at the same level of theory to reinforce the ground state structures and to take into account the zero-point energy correction.

4. RESULTS AND DISCUSSION

4.1. Photoelectron Imaging Spectroscopy of ZrC_2^-. The photoelectron image and the corresponding photoelectron spectrum of ZrC_2^- acquired at 2.33 eV photon energy is presented in Figure 1. The double yellow arrow in the photoelectron image indicates the direction of laser polarization, which is vertical in the image plane. Many rings can be observed in the photoelectron image, which correspond to different peaks in the related photoelectron spectrum. As shown in Figure 1, the 532 nm spectrum of ZrC_2^- reveals two prominent transition bands, labeled X and A. The band X represents the electron affinity (EA) defining transition, resulting from the transition between the electronic ground state of ZrC_2^- and its corresponding neutral ground state. The vertical detachment energy (VDE) of this band is measured to be 1.67 ± 0.09 eV from the band maximum. As can be seen from Figure 1, there exist vibrational structures in band X. Careful inspection of the peak positions reveals two vibrational progressions for this band, which are 564.6 and 1774.0 cm^{-1}, respectively. Furthermore, according to the vibrationally resolved PES, the adiabatic detachment energy (ADE) of ZrC_2^- is determined to be about 1.60 ± 0.07 eV, which is also the EA of ZrC_2 neutral. Additionally, as presented in the photoelectron image, transition X displays a preferably parallel photoelectron angular distribution (PAD) with respect to the laser polarization, and an anisotropy parameter (β) of 1.25 ± 0.02 is obtained for the most intense peak in transition X, which may imply that the detachment process more likely occurs from a molecular orbital composed mainly of the *s*-type character.[35,36,50] Another feature appears in the higher binding energy region, beginning from about 2.00 to 2.33 eV, of the figure, and we temporarily assign it as A. It seems that there are several resolved peaks in this band, which are also consistent with the inner rings located in the photoelectron image (Figure 1). These peaks probably stem from the removal of deeper lying electrons giving rise to the neutral cluster in vibrationally or electronically excited states. Precise assignment of these peaks requires higher-level ab initio theoretical methods considering the excited states of the clusters, which is beyond the scope and the focus of the current study.

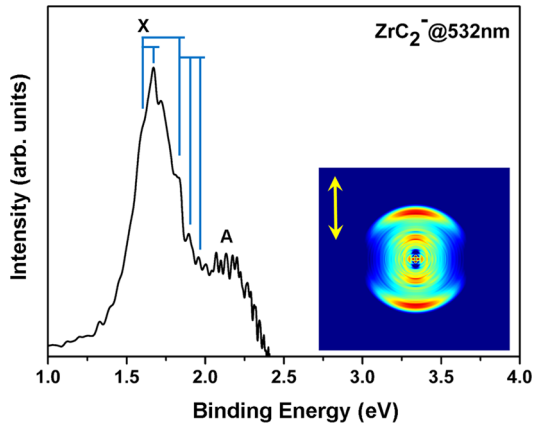

Figure 1. Photoelectron image and the corresponding electron binding energy (eBE) spectrum of the ZrC_2^- cluster as measured with 532 nm photon energy.

4.2. Theoretical Results on the Optimized Geometries of Anionic and Neutral ZrC_2. To better understand the electronic structures of the $ZrC_2^{0/-1}$ clusters, high-level theoretical calculations have been accomplished to explore the optimized geometries of the clusters. Various initial geometries and spin states were attempted to determine the

dx.doi.org/10.1021/jp505648u | J. Phys. Chem. A 2014, 118, 6935−6939

lowest energy structures of the anionic and neutral ZrC_2 clusters. Specifically, four possible geometries for these three-atom clusters were considered, including the triangular structure, the bent structure, and two linear ones, which are Zr−C−C and C−Zr−C structures. Figure 2 depicts the lowest

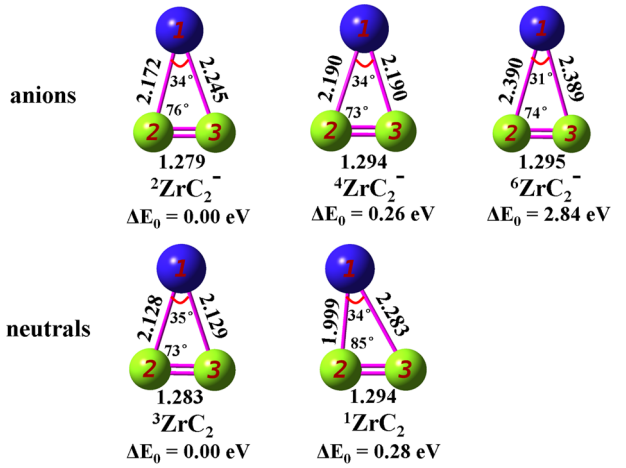

Figure 2. Optimized geometries of the anionic and neutral ZrC_2 clusters calculated at the CCSD(T) level of theory. Bond lengths are given in angstroms, and the superscripts present spin multiplicity. The relative energies ΔE_0 with respect to the ground state are shown in units of eV (the subscript zero indicates the application of the zero-point energy correction in the present calculations). The blue spheres represent Zr atoms, while the green spheres correspond to C atoms.

energy geometries of the $ZrC_2^{0/-1}$ clusters as well as some selected low-lying isomers obtained at the present CCSD(T) level of theory. As shown in Figure 2, the ground state of ZrC_2^- has a bent structure with the bond lengths of two Zr−C bonds being 2.172 and 2.245 Å, respectively. The spin multiplicity for the lowest-energy structure is 2, while the quartet and sextet states are 0.26 and 2.84 eV, respectively, higher in energy calculated at the present level of theory. In the case of neutral ZrC_2, the lowest energy geometry exhibits a triangular C_{2v} structure. The Zr−C and C−C bond lengths are calculated to be about 2.128 and 1.283 Å, respectively. According to the present theoretical calculations, the ground state of the neutral ZrC_2 cluster shows a higher triplet state, which is more stable than the singlet-state structure by 0.28 eV. Note that there is a geometric distortion for the singlet-state isomer with respect to the ground state $^3ZrC_2$, which makes the $^1ZrC_2$ isomer have a bent structure, as shown in Figure 2.

4.3. Comparison between Experiment and Theory. To validate the lowest energy structures of the anionic and neutral ZrC_2 clusters (Figure 2), the theoretical ADE and VDE of ZrC_2^- were calculated at the present level of theory, which can be used to compare with the experimental values. The theoretical ADE was obtained by calculating the energy difference between the anionic and neutral ground states, while the calculated VDE was estimated as the energy difference between the ground-state geometry of the anion and the neutral cluster without geometrical change with respect to the anionic ground state. The calculated results are listed in Table 1 as well as the electron configurations and vibrational frequencies of the studied clusters. As shown in Table 1, theoretical ADE and VDE of the ZrC_2^- cluster are 1.52 and 1.66 eV calculated at the present CCSD(T) level of theory, respectively, which are in good agreement with the experimentally measured values. Additionally, as mentioned earlier, the electron affinity defined peak (transition X) in Figure 1 displays vibrational structures, yielding vibrational frequencies of ∼564.6 and ∼1774.0 cm^{-1} (Table 1). According to the present theoretical calculations, the vibrational frequencies of the symmetric Zr−C_2 and C−C stretching modes of the neutral ZrC_2 cluster are calculated to be about 597.0 and 1741.1 cm^{-1}, respectively, which are consistent with the experimental data. Therefore, all the findings discussed above provide evidence that our optimized ground-state structures of the anionic and neutral ZrC_2 clusters, as depicted in Figure 2, are correct.

4.4. Molecular Orbitals and Chemical Bonding. Having determined the optimized geometries of the anionic and neutral ZrC_2 clusters, we endeavor to shed light on their molecular orbitals (MOs) and chemical bonding. Figure 3 displays the occupied valence MOs of the clusters. According to our theoretical calculations, neutral ZrC_2 is a polar molecule since its dipole moment is calculated to be about 6.10 D. The atomic charges, determined from the Mulliken population analysis, are +0.38, −0.19, and −0.19 for the metal atom (Zr) and two C atoms, respectively. This charge distribution is in line with the relative electronegativities of Zr and C. Therefore, the interaction between Zr and C_2 in the neutral ZrC_2 cluster can be viewed as ionic, which is similar to that of other transition metal dicarbides.[16,51] As shown in Figure 3, the HOMO and HOMO−1 of ZrC_2 are singly occupied molecular orbitals (SOMOs). The HOMO is formed primarily by the sd_z^2-type hybrid orbital on Zr, whose distribution of the electron cloud is similar to that of the ZrO_2^- cluster,[52] while the HOMO−1 is mainly composed of the $4d_{xz}$-AO on Zr. In addition, there are two delocalized MOs in the neutral cluster,

Table 1. Experimental and Theoretical ADE and VDE, in Units of eV, of the ZrC_2^- Cluster and Experimental Vibrational Frequencies (cm^{-1}) for the Neutral ZrC_2 Cluster

		ADE		VDE		ν_e	
species	electron configuration[a]	exptl	theor	exptl	theor	exptl	theor[b]
$^2ZrC_2^-$	...$(1a')^2(2a')^2(3a')^2(1a'')^2(4a')^2(2a'')^1(5a')^2$	1.60(7)	1.52	1.67(9)	1.66		632.1
							926.3
							1999.8
$^3ZrC_2$	...$(1a')^2(2a')^2(3a')^2(1a'')^2(4a')^2(2a'')^1(5a')^1$						140.0
						564.6	597.0
						1774.0	1741.1

[a]Calculated electron configurations of the anionic and neutral ZrC_2 clusters. [b]Theoretical vibrational frequencies of the anionic and neutral ZrC_2 clusters.

dx.doi.org/10.1021/jp505648u | J. Phys. Chem. A 2014, 118, 6935−6939

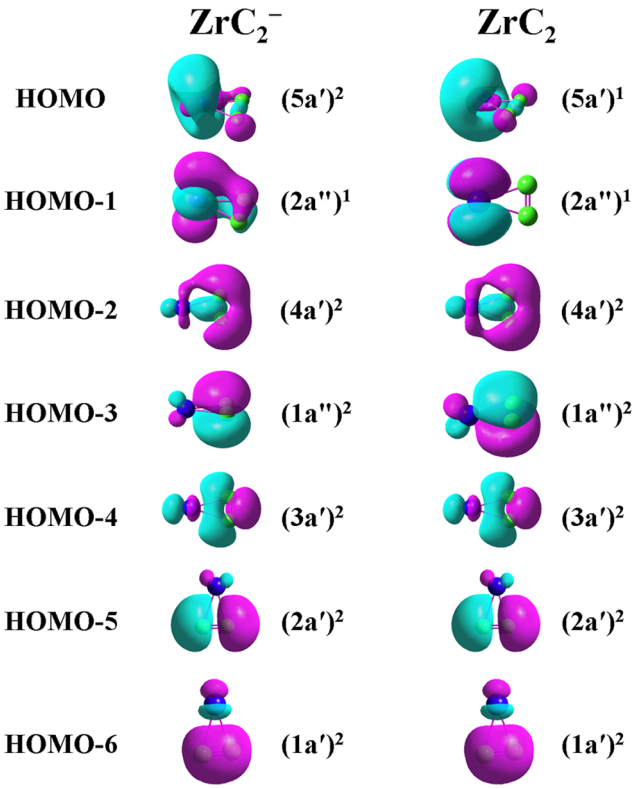

Figure 3. Occupied valence molecular orbitals (MOs) of the anionic and neutral ZrC_2 clusters. The isosurface value of the MOs is 0.03 au.

which are HOMO−2 and HOMO−3. HOMO−2 is a σ-type delocalized MO consisting of the overlap of the Zr $4d_{x^2-y^2}$ and the P_σ-radial orbitals on another two carbon atoms, and HOMO−3 is a π-type delocalized MO resulting from the overlap between the $4d_{yz}$ AO on Zr and the P_π orbitals from the remaining carbon atoms. Other MOs in ZrC_2, namely, HOMO−4, HOMO−5, and HOMO−6, are localized MOs, which are similar to the lowest three valence MOs in LaB_3.[36] As for forming the anionic ZrC_2 cluster, the extra electron can occupy one of the SOMOs of neutral ZrC_2, which are HOMO or HOMO−1 in ZrC_2, to produce the doublet ground-state ZrC_2^-. According to our theoretical calculations, as shown in Figure 3, the excess electron occupies the singly occupied 5a′ state of ZrC_2 that mainly comprises the sd_z^2 hybrid orbital on Zr. Note that this finding is also qualitatively consistent with our measured β value (1.25 ± 0.02), as mentioned earlier, which may imply that the detachment process more likely occurs from a molecular orbital composed mainly of the s-type character.

5. CONCLUSIONS

In summary, the electronic and geometrical properties of the anionic and neutral ZrC_2 clusters were examined using a synergistic approach combining photoelectron imaging spectroscopy and high-level theoretical calculations. A photoelectron spectrum with apparent vibrational structures was reported at 532 nm photon energy, from which the experimental electron affinity of neutral ZrC_2 was measured to be 1.60 ± 0.07 eV. The vibrational structures in the PES disclose two vibrational frequencies of the neutral cluster, which are 564.6 and 1774.0 cm^{-1}, respectively, and they are attributed to the symmetric Zr−C_2 and C−C stretching modes based on the theoretical calculations. In addition, the Mulliken population and molecular orbitals were calculated to explore the electronic structures and nature of the chemical bonding of the clusters. The interaction between Zr and C_2 in neutral ZrC_2 is found to be ionic, and the extra electron in ZrC_2^- occupies an sd_z^2 hybrid orbital located on the Zr atom.

AUTHOR INFORMATION

Corresponding Author

*(A.W.C.) Tel: (814)865-7242. Fax: (814)865-5235. E-mail: awc@psu.edu.

Notes

The authors declare no competing financial interest.

ACKNOWLEDGMENTS

This material is based upon work supported by the Air Force Office of Science Research under AFOSR Award No. FA9550-10-1-0071.

REFERENCES

(1) Clemmer, D. E.; Hunter, J. M.; Shelimov, K. B.; Jarrold, M. F. Physical and Chemical Evidence for Metallofullerenes with Metal Atoms as Part of the Cage. *Nature* **1994**, *372*, 248−250.

(2) Shinohara, H. Endohedral Metallofullerenes. *Rep. Prog. Phys.* **2000**, *63*, 843−892.

(3) Guo, B. C.; Kerns, K. P.; Castleman, A. W., Jr. $Ti_8C_{12}^+$-Metallo-carbohedrenes: A New Class of Molecular Clusters. *Science* **1992**, *255*, 1411−1413.

(4) Guo, B. C.; Wei, S.; Purnell, J.; Buzza, S.; Castleman, A. W., Jr. Metallo-carbohedrenes [$M_8C_{12}^+$ (M = V, Zr, Hf, and Ti)]: A Class of Stable Molecular Cluster Ions. *Science* **1992**, *256*, 515−516.

(5) Wei, S.; Guo, B. C.; Purnell, J.; Buzza, S.; Castleman, A. W., Jr. Metallo-carbohedrenes: Formation of Multicage Structures. *Science* **1992**, *256*, 818−820.

(6) Iijima, S.; Ichihashi, T. Single-shell Carbon Nanotubes of 1-nm Diameter. *Nature* **1993**, *363*, 603−605.

(7) Guo, B. C.; Kerns, K. P.; Castleman, A. W., Jr. Reactivities of $Ti_8C_{12}^+$ at Thermal Energies. *J. Am. Chem. Soc.* **1993**, *115*, 7415−7418.

(8) Cartier, S. F.; May, B. D.; Castleman, A. W., Jr. Binary Metal Metallocarbohedrenes of Titanium and Group IIIA, VA, and VIA Metals. *J. Am. Chem. Soc.* **1994**, *116*, 5295−5297.

(9) Cartier, S. F.; May, B. D.; Castleman, A. W., Jr. $Ti_xZr_yC_{12}$ and $Ti_xHf_yC_{12}$ (x + y = 8): Binary Metal Metallocarbohedrenes. *J. Chem. Phys.* **1994**, *100*, 5384−5386.

(10) Cartier, S. F.; May, B. D.; Castleman, A. W., Jr. The delayed Ionization and Atomic Ion Emission of Binary Metal Metallocarbohedrenes $Ti_xM_yC_{12}$ (M = Zr, Nb; 0 ≤ y ≤ 4; x + y = 8). *J. Chem. Phys.* **1996**, *104*, 3423−3432.

(11) van Heijnsbergen, D.; von Helden, G.; Duncan, M. A.; van Roij, A. J. A.; Meijer, G. Vibrational Spectroscopy of Gas-phase Metal-carbide Clusters and Nanocrystals. *Phys. Rev. Lett.* **1999**, *83*, 4983−4986.

(12) Pilgrim, J. S.; Duncan, M. A. Metallo-Carbohedrenes: Chromium, Iron, and Molybdenum Analogs. *J. Am. Chem. Soc.* **1993**, *115*, 6958−6961.

(13) Rohmer, M. M.; Bénard, M.; Poblet, J. M. Structure, Reactivity, and Growth Pathways of Metallocarbohedrenes M_8C_{12} and Transition Metal/Carbon Clusters and Nanocrystals: A Challenge to Computational Chemistry. *Chem. Rev.* **2000**, *100*, 495−542.

(14) Reddy, B. V.; Khanna, S. N.; Jena, P. Electronic, Magnetic, and Geometric Structure of Metallo-Carbohedrenes. *Science* **1992**, *258*, 1640−1643.

(15) Hwu, H. H.; Chen, J. G. Surface Chemistry of Transition Metal Carbides. *Chem. Rev.* **2005**, *105*, 185−212 and references therein..

(16) Li, X.; Wang, L. S. Electronic Structure and Chemical Bonding between the First Row Transition Metals and C_2: A Photoelectron

Spectroscopy Study of MC_2^- (M=Sc, V, Cr, Mn, Fe, and Co). *J. Chem. Phys.* **1999**, *111*, 8389−8395.
(17) Yuan, J. Y.; Xu, H. G.; Zheng, W. J. Photoelectron Spectroscopy and Density Functional Study of $Co_nC_2^-$ (n = 1−5) clusters. *Phys. Chem. Chem. Phys.* **2014**, *16*, 5434−5439.
(18) Rayón, V. M.; Redondo, P.; Barrientos, C.; Largo, A. Structure and Bonding in First-row Transition-metal Dicarbides: Are They Related to the Stability of Met-cars? *Chem.—Eur. J.* **2006**, *12*, 6963−6975.
(19) Gutsev, G. L.; Andrews, L.; Bauschlicher, C. W. Similarities and Differences in the Structure of 3*d*-metal Monocarbides and Monoxides. *Theor. Chem. Acc.* **2003**, *109*, 298−308.
(20) Ticknor, B. W.; Bandyopadhyay, B.; Duncan, M. A. Photodissociation of Noble Metal-Doped Carbon Clusters. *J. Phys. Chem. A* **2008**, *112*, 12355−12366.
(21) Rayón, V. M.; Redondo, P.; Barrientos, C.; Largo, A. Structure and Bonding in First-row Transition Metal Dicarbide Cations MC_2^+. *J. Phys. Chem. A* **2007**, *111*, 6345−6353.
(22) Langenberg, J. D.; Shao, L.; Morse, M. D. Resonant Two-photon Ionization Spectroscopy of Jet-cooled PdC. *J. Chem. Phys.* **1999**, *111*, 4077−4086.
(23) Wang, Y.; Szczepanski, J.; Vala, M. Silver-carbon Cluster AgC_3: Structure and Infrared Frequencies. *J. Phys. Chem. A* **2008**, *112*, 11088−11092.
(24) Zhai, H. J.; Liu, S. R.; Li, X.; Wang, L. S. Photoelectron Spectroscopy of Mono-niobium Carbide Clusters NbC_n^- (n = 2−7): Evidence for a Cyclic to Linear Structural Transition. *J. Chem. Phys.* **2001**, *115*, 5170−5178.
(25) Clayborne, P. A.; Jones, C. E., Jr.; Gupta, U.; Melko, J. J.; Khanna, S. N.; Castleman, A. W., Jr. Structural Evolution of Triniobium Carbide Clusters: Evidence of Large C_n Chains (n = 3−4) in $Nb_3C_n^-$ (n = 5−10) Clusters. *J. Phys. Chem. A* **2010**, *114*, 1290−1297.
(26) Knappenberger, K. L., Jr.; Clayborne, P. A.; Reveles, J. U.; Sobhy, M. A.; Jones, C. E., Jr.; Gupta, U. U.; Khanna, S. N.; Iordanov, I.; Sofo, J.; Castleman, A. W., Jr. Anion Photoelectron Spectroscopy and Density Functional Investigation of Diniobium-carbon Clusters. *ACS Nano* **2007**, *1*, 319−326.
(27) Sanov, A.; Lineberger, W. C. Cluster Anions: Structure, Interactions, and Dynamics in the Sub-nanoscale Regime. *Phys. Chem. Chem. Phys.* **2004**, *6*, 2018−2032.
(28) Melko, J. J.; Werner, U.; Mitrić, R.; Bonačić-Koutecký, V.; Castleman, A. W., Jr. Electronic Structure Similarities in $Pb_xSb_y^-$ and $Sn_xBi_y^-$ Clusters. *J. Phys. Chem. A* **2011**, *115*, 10276−10280.
(29) Liu, B.; Long, T.; Wang, Y.; Wang, L. Femtosecond Photodetachment of Silver Anions. *J. Phys. Chem. A* **2013**, *117*, 11210−11216.
(30) Cheng, S. B.; Berkdemir, C.; Melko, J. J.; Castleman, A. W., Jr. S-P Coupling Induced Unusual Open-Shell Metal Clusters. *J. Am. Chem. Soc.* **2014**, *136*, 4821−4824.
(31) Berkdemir, C.; Cheng, S. B.; Castleman, A. W., Jr. Assigning the Mass Spectrum of NbN^-: Photoelectron Imaging Spectroscopy and Nominal-mass Counterpart Analysis. *Int. J. Mass Spectrom.* **2014**, *365*−*366*, 222−224.
(32) Wu, X.; Xie, H.; Qin, Z. B.; Tan, K.; Tang, Z. C.; Lu, X. Photoelectron Imaging and Theoretical Studies of Silver Monohalides AgX^- (X = Cl, Br, I) and $AuCl^-$. *J. Phys. Chem. A* **2011**, *115*, 6321−6326.
(33) Yandell, M. A.; King, S. B.; Neumark, D. M. Time-Resolved Radiation Chemistry: Photoelectron Imaging of Transient Negative Ions of Nucleobases. *J. Am. Chem. Soc.* **2013**, *135*, 2128−2131.
(34) Grubisic, A.; Ko, Y. J.; Wang, H. P.; Bowen, K. H. Photoelectron Spectroscopy of Lanthanide-Silicon Cluster Anions $LnSi_n^-$ ($3 \leq n \leq 13$; Ln = Ho, Gd, Pr, Sm, Eu, Yb): Prospect for Magnetic Silicon-Based Clusters. *J. Am. Chem. Soc.* **2009**, *131*, 10783−10790.
(35) Peppernick, S. J.; Gunaratne, K. D. D.; Castleman, A. W., Jr. Superatom Spectroscopy and the Electronic State Correlation between Elements and Isoelectronic Molecular Counterparts. *Proc. Natl. Acad. Sci. U.S.A.* **2010**, *107*, 975−980.
(36) Cheng, S. B.; Berkdemir, C.; Castleman, A. W., Jr. Observation of d-p Hybridized Aromaticity in Lanthanum-doped Boron Clusters. *Phys. Chem. Chem. Phys.* **2014**, *16*, 533−539.
(37) Cheng, S.; Berkdemir, C.; Melko, J. J.; Castleman, A. W., Jr. Probing the Electronic Structures and Relative Stabilities of Monomagnesium Oxide Clusters MgO_x^- and MgO_x (x = 1−4): A Combined Photoelectron Imaging and Theoretical Investigation. *J. Phys. Chem. A* **2013**, *117*, 11896−11905.
(38) Knappenberger, K. L.; Jones, C. E.; Sobhy, M. A.; Castleman, A. W., Jr. Versatile Cluster Based Photoelectron Spectrometer. *Rev. Sci. Instrum.* **2006**, *77*, 123901.
(39) Sobhy, M. A.; Reveles, J. U.; Gupta, U.; Khanna, S. N.; Castleman, A. W., Jr. Photoelectron Imaging and Theoretical Investigation of Bimetallic $Bi_{1-2}Ga_{0-2}^-$ and Pb_{1-4}^- Cluster Anions. *J. Chem. Phys.* **2009**, *130*, 054304.
(40) Wiley, W. C.; McLaren, I. H. Time-of-Flight Mass Spectrometer with Improved Resolution. *Rev. Sci. Instrum.* **1955**, *26*, 1150−1157.
(41) Dribinski, V.; Ossadtchi, A.; Mandelshtam, V. A.; Reisler, H. Reconstruction of Abel-transformable Images: The Gaussian Basis-set Txpansion Abel Transform Method. *Rev. Sci. Instrum.* **2002**, *73*, 2634−2642.
(42) Garcia, G. A.; Nahon, L.; Powis, I. Two-dimensional Charged Particle Image Inversion Using a Polar Basis Function Expansion. *Rev. Sci. Instrum.* **2004**, *75*, 4989−4996.
(43) Andersen, T.; Haugen, H. K.; Hotop, H. Binding Energies in Atomic Negative Ions: III. *J. Phys. Chem. Ref. Data* **1999**, *28*, 1511−1533.
(44) Frisch, M. J.; Trucks, G. W.; Schlegel, H. B.; Scuseria, G. E.; Robb, M. A.; Cheeseman, J. R.; Scalmani, G.; Barone, V.; Mennucci, B.; Petersson, G. A.; et al. *Gaussian 09*, revision A.1; Gaussian, Inc.: Wallingford, CT, 2009.
(45) Purvis, G. D., III; Bartlett, R. J. A Full Coupled-cluster Singles and Doubles Model: the Inclusion of Disconnected Triples. *J. Chem. Phys.* **1982**, *76*, 1910−1918.
(46) Raghavachari, K.; Trucks, G. W.; Pople, J. A.; Head-Gordon, M. A Fifth-order Perturbation Comparison of Electron Correlation Theories. *Chem. Phys. Lett.* **1989**, *157*, 479−483.
(47) Dunning, T. H., Jr. Gaussian Basis Sets for use in Correlated Molecular Calculations. I. The Atoms Boron through Neon and Hydrogen. *J. Chem. Phys.* **1989**, *90*, 1007−1023.
(48) Kendall, R. A.; Dunning, T. H., Jr.; Harrison, R. J. Electron Affinities of the First-row Atoms Revisited. Systematic Basis Sets and Wave Functions. *J. Chem. Phys.* **1992**, *96*, 6796−6806.
(49) Peterson, K. A.; Figgen, D.; Dolg, M.; Stoll, H. Energy-consistent Relativistic Pseudopotentials and Correlation Consistent Basis Sets for the 4d Elements Y−Pd. *J. Chem. Phys.* **2007**, *126*, 124101.
(50) Wenthold, P. G.; Gunion, R. F.; Lineberger, W. C. Ultraviolet Negative-ion Photoelectron Spectroscopy of the Chromium Oxide Negative Ion. *Chem. Phys. Lett.* **1996**, *258*, 101−106.
(51) Dai, D.; Roszak, S.; Balasubramanian, K. Electronic States and Potential Energy Surfaces of NbC_2. *J. Phys. Chem. A* **2000**, *104*, 5861−5866.
(52) Zheng, W. J.; Bowen, K. H.; Li, J.; Dabkowska, I.; Gutowski, M. Electronic Structure Differences in ZrO_2 vs HfO_2. *J. Phys. Chem. A* **2005**, *109*, 11521−11525.